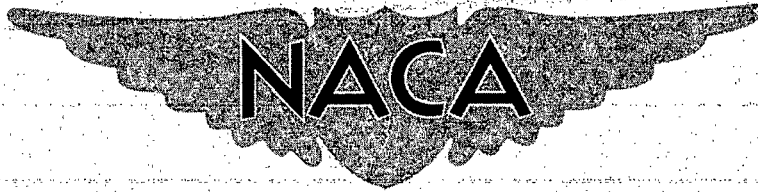


CONFIDENTIAL

Copy 6
RM L56E07

C 2



RESEARCH MEMORANDUM

NOT TO BE TAKEN FROM THIS ROOM

SOME EXPERIMENTS RELATING TO THE PROBLEM OF SIMULATION OF
HOT JET ENGINES IN STUDIES OF JET EFFECTS ON ADJACENT
SURFACES AT A FREE-STREAM MACH NUMBER OF 1.80

By Walter E. Bressette

Langley Aeronautical Laboratory
Langley Field, Va.

CLASSIFICATION CHANGES

UNCLASSIFIED

authority of *NASA TPA 9* Date *9-1-59* *Effective*

NB 12-21-59

CLASSIFIED DOCUMENT

This material contains information affecting the National Defense of the United States within the meaning of the espionage laws, Title 18, U.S.C., Secs. 793 and 794, the transmission or revelation of which in any manner to an unauthorized person is prohibited by law.

NATIONAL ADVISORY COMMITTEE FOR AERONAUTICS

WASHINGTON

July 11, 1956

CONFIDENTIAL

UNCLASSIFIED



NATIONAL ADVISORY COMMITTEE FOR AERONAUTICS

RESEARCH MEMORANDUM


SOME EXPERIMENTS RELATING TO THE PROBLEM OF SIMULATION OF
HOT JET ENGINES IN STUDIES OF JET EFFECTS ON ADJACENT
SURFACES AT A FREE-STREAM MACH NUMBER OF 1.80

By Walter E. Bressette

SUMMARY

An investigation at a free-stream Mach number of 1.80 in a blowdown-type tunnel was made to study the effect on the pressure distribution of a zero-angle-of-attack wing surface when certain exhaust parameters of a hot turbojet engine are varied. Static-pressure surveys were made on a wing surface that was located in the vicinity of a small-scale propulsive jet. This propulsive jet was operated with four types of jet exhausts. These jet exhausts were a hot jet (hydrogen burned in air), a cold air jet, a cold helium jet, and a jet composed of a mixture of two cold gases (hydrogen and carbon dioxide). The hot jet, because of its high exhaust temperature ($3,300^{\circ}\text{R}$) and because combustion was performed in air, was believed reasonably able to simulate the exhaust parameters of an actual afterburning turbojet engine. The cold jets used were selected in order that the effects of a variation in the exhaust parameters of jet-exit static-pressure ratio, ratio of specific heats, density, and velocity, could be obtained by comparing each cold jet with the hot jet or with another cold jet. The tests were made over a range of jet-exit static-pressure ratios from 1 to 9 with values of the ratio of specific heats of 1.27, 1.40, and 1.66 and at variations in density and velocity of the order of approximately 8 and 3 times, respectively.

Within the scope of this investigation, it was found that jet-exit static-pressure ratio and the ratio of specific heats affected the pressure distribution on the wing associated with jet interference while a variation in exit velocity and density did not. The jet-exit static-pressure ratio affected the wing pressure distribution in a major way while the ratio of specific heats had only a minor effect. The addition of temperature in the propulsive jet exhaust at a jet-exit static-pressure ratio of 4 had little or no effect on the pressure distribution associated with jet interference on the wing.



INTRODUCTION

It has been shown in references 1 to 3 that a propulsive jet issuing from the rear of a nacelle into free-stream supersonic flow causes jet effects on parallel surfaces located in the near vicinity and downstream of the propulsive jet exit. The results of references 1 and 3 were obtained with a cold helium propulsive jet, whereas in reference 2 a cold air jet was used. Naturally the use of these cold jets raises the question of how comparative are the results obtained from a cold jet in relation to the results that would be obtained from a hot exhaust from a jet engine. It is well known that the presence of additional heat in the propulsive jet will influence the exhaust parameters of pressure, density, ratio of specific heats, and velocity. When a cold propulsive jet is used, it is impossible to duplicate all the exhaust parameters of a hot jet at the same time because, while the pressure of the cold jet may be varied, the temperature and the exhaust parameters influenced by the temperature alone must remain essentially constant. Therefore, it is important to know just how each of these exhaust parameters affects the physical characteristics of the propulsive jet exhaust and its subsequent effect on the pressure data obtained as in references 1 to 3. A theoretical analysis showing the effect of both pressure and the ratio of specific heats on the physical characteristics of the exhaust jet was made in reference 4 and some experimental jet-effect data involving both of these parameters are shown in reference 3.

The investigation was conducted in the preflight jet of the Langley Pilotless Aircraft Research Station at Wallops Island, Va., by using a small-scale nacelle simulating a turbojet nacelle that was located beneath a flat surface simulating a wing. The small-scale nacelle with a sonic exit was operated with a hot jet (hydrogen burned in air), a cold air jet, a cold helium jet, and a jet composed of a mixture of two cold gases (carbon-dioxide and hydrogen). From the resulting pressure distributions as measured on the wing for each of the cold exhaust jets as compared with the hot jet or with another cold jet, the influence of pressure and the ratio of specific heats as well as temperature, density, and velocity on the jet effects upon adjacent surfaces was obtained.

SYMBOLS

C_p pressure coefficient, $\frac{p_w - p_\infty}{q_\infty}$

D diameter, in.

M	Mach number
p	static pressure, lb/sq in.
p'	total pressure, lb/sq in.
$\frac{p_c'}{p_\infty}$	nacelle-chamber total-pressure ratio
$\frac{p_j}{p_\infty}$	jet-exit static-pressure ratio
$\frac{p_j'}{p_\infty}$	jet-exit total-pressure ratio
q	dynamic pressure, $\frac{\gamma p M^2}{2}$, lb/sq in.
R	gas constant, $\frac{\text{ft-lb}}{\text{lb } ^\circ\text{R}}$
T	absolute temperature, $^\circ\text{R}$
x	chordwise distance from nacelle exit (downstream is positive), in.
y	spanwise distance from nacelle center line, in.
γ	ratio of specific heat at constant pressure to specific heat at constant volume
θ	inclination of exit shock with respect to nacelle center line, deg
ρ	density, lb/cu ft
V	velocity, ft/sec
$\text{H}_2 + \text{CO}_2$	propulsive jet composed of a mixture of hydrogen and carbon dioxide

Subscripts:

j	jet exit
f	propulsive jet off
n	propulsive jet on

w wing
 ∞ free stream

APPARATUS

The tests were made in the preflight jet of the Langley Pilotless Aircraft Research Station at Wallops Island, Va. (described in ref. 5). A Mach number 1.80, 27- by 27-inch nozzle was used for all tests. A photograph of the nacelle mounted in the test position beneath the flat-surface wing at the exit of the 27- by 27-inch nozzle is shown as figure 1.

A sketch of the nacelle with its principal dimensions is shown in figure 2 and the location of the nacelle with respect to the wing and exit of the preflight-jet nozzle is presented in figure 3. The choice of nacelle position was made by determining which position in reference 3 gave the best shadowgraph pictures in relation to the pressure rise on the wing from the jet. The nacelle was designed to produce a hot propulsive jet (hydrogen burned in air) or a cold propulsive jet by exhausting any type of pressurized gas fed in through the supply line. All details of the nacelle and wing, as well as the instrumentation used in these tests, were identical with those of reference 3 and are discussed in detail there.

The positions of 47 static-pressure orifices on the wing with respect to the nacelle exit are shown in figure 4.

TEST AND METHODS

The tests were made at a free-stream Mach number of 1.80 with a Reynolds number per foot of approximately 13×10^6 . The nacelle exit was located as shown in figure 3.

The equipment was designed to permit tests with the nacelle operating with various types of sonic propulsive jets as follows:

(1) A hot jet (hydrogen burned in air) having an exhaust temperature (3,300° R) which is closely comparable to an actual afterburning turbojet engine (fig. 3, ref. 6). Therefore, it is believed that the exhaust parameters of density, γ , and velocity of this hot jet are similar to those for an actual afterburning turbojet engine at the same value of p_j/p_∞ .

(2) A cold air jet for which p_j/p_∞ could be varied, while having fixed values of density, γ , and velocity which were different than those for the hot jet.

(3) A cold helium jet for which p_j/p_∞ could be varied, while having fixed values of density, γ , and velocity. The density and velocity of this jet were similar to the hot jet while the value of γ was different from the value for both the air jet and the hot jet.

(4) A cold jet composed of a mixture of hydrogen and carbon dioxide for which p_j/p_∞ could be varied, while having fixed values of density, γ , and velocity. The density and velocity of this jet were similar to both the hot jet and the helium jet while γ was similar to the air jet.

The variation in p_j/p_∞ with p_j'/p_∞ for each of the cold jets is presented in figure 5 and the values of density, γ , and velocity for each of the jets tested are presented in table I.

A high-frequency strain-gage balance was used to measure both the total drag (nacelle jet-off) and the net thrust (nacelle jet-on). The gross thrust was then obtained by an algebraic summation of these measurements. The static pressure at the exit of the nacelle was calculated from the gross thrust by the method as presented in reference 3. A nacelle static pressure was measured for all test runs as well as a total pressure for all cold test runs. (See fig. 2.) The variation of measured nacelle-chamber total-pressure ratio with calculated jet-exit total-pressure ratio (from thrust measurements) for the cold jets tested is presented in figure 6.

ACCURACY

By accounting for the instrument error of 1 percent of full-scale range, the probable error is believed to be within the following limits:

M	±0.02
C_{p_f}	±0.02
C_{p_n}	±0.02
p_j/p_∞	±0.05
p_j'/p_∞	±0.05

RESULTS AND DISCUSSION

Shock Waves

Presented in figure 7 are typical shadowgraph pictures of the flow field about the nacelle exit for the four types of propulsive jets tested. Clearly visible, downstream of the nacelle exit, in each of the pictures presented in figure 7 are two shock waves that impinge upon the wing surface and then are reflected. In keeping with the nomenclature of reference 4, the first of these shock waves will be called the exit shock and the second will be called the jet shock. In the theoretical investigation of reference 4, it is shown that both the exhaust parameters of static pressure ratio and γ will determine the initial inclination of the jet boundary from a sonic exit and, therefore, the shape of the exhaust jet. This exhaust shape when acting in conjunction with stream Mach number will determine the angles and, therefore, the strength and intersecting points on the flat plate wing of the two shock waves visible in figure 7. These intersecting points as determined from shadowgraph pictures for all the propulsive jets tested are presented in figure 8 plotted as the variation of chordwise distance downstream of the nacelle exit in jet-exit diameters with jet-exit static-pressure ratio. Figure 8 shows that as p_j/p_∞ is increased, the point of intersection on the wing of the exit shock moves toward the nacelle exit while the point of intersection on the wing of the jet shock moves away from the nacelle exit. This movement is accomplished in the case of the exit shock by an increase in angle of inclination as shown in figure 9. For the jet shock, however, the downstream movement of the intersecting point was related to a downstream movement of the jet shock. Figure 8 also shows that within the accuracy of shadowgraph measurements, the variation of x/D_j with p_j/p_∞ is essentially the same for all the propulsive jets tested. This fact indicates that the jet-exit static-pressure ratio parameter is the major parameter affecting the shock pattern in these tests and that the other exhaust parameters as outlined in table I may be expected to have a minor effect.

Pressure Coefficients

In order to determine which orifice locations were influenced by the intersection on the wing of either the exit shock or the jet shock in these tests, a simple conical projection of the exit shock was made by using the angles as presented in figure 9 at p_j/p_∞ of 1.5 and 9. The results of these projections are shown in figure 10. The jet shock influences only those orifices that are located downstream of the intersection of the exit shock at p_j/p_∞ of 1.5. Naturally, the orifices

located between the lines of intersection of the exit shock at $p_j/p_\infty = 1.5$ and $p_j/p_\infty = 9$ are influenced by the exit shock. All other orifices that were located ahead of the intersection of the exit shock at $p_j/p_\infty = 9$ had the same value of pressure coefficient whether the propulsive jet was on or off. The values of jet-off pressure coefficients for all orifices are presented in table II.

Effect of jet properties on exit-shock pressure coefficients.-

Presented in figure 11 is the variation of C_{p_n} with p_j/p_∞ influenced by the exit shock at each of the wing pressure orifices for all the propulsive jets tested. Typical curves taken from the data of figure 11 for the orifices located at $x/D_j = 3.47$ are presented in figure 12 for the purpose of discussion. The rapid C_{p_n} rise at each of the stationary orifice positions in figure 12 happens when the point of intersection of the exit shock on the wing passes over the orifice as it moves upstream when p_j/p_∞ is increased. Figure 12 also shows that the rapid C_{p_n} rise occurs at approximately the same values of p_j/p_∞ for both the air and the $H_2 + CO_2$ jets whereas it occurs at higher values of p_j/p_∞ for the helium jet. This difference in C_{p_n} rise must be an effect of γ on the location of the exit shock because, as shown in table I, the air jet and the $H_2 + CO_2$ jet, which agree in C_{p_n} rise, have approximately the same values of γ whereas density and exit velocity are decidedly different. In addition, the helium jet, which does not agree in C_{p_n} rise, has approximately the same values of density and exit velocity as the $H_2 + CO_2$ jet but the value of γ is different from the common value for both the air and the $H_2 + CO_2$ jets. The greater difference in the variation of C_{p_n} in figure 12(b) between the helium jet and the air and $H_2 + CO_2$ jets tested as compared with figure 12(a) indicates that the effect of γ on the location of the exit shock is an increasing one with an increase in p_j/p_∞ . This influence of γ on the exit shock is also shown in the theoretical investigation of reference 4 as well as in the experimental investigation of reference 3. From the results of these tests as presented in figures 11 and 12, it appears that both p_j/p_∞ and γ will affect C_{p_n} as influenced by the exit shock while the exhaust parameters of density and velocity do not.

Effect of jet properties on jet shock pressure coefficients.-
Presented in figure 13 is the variation of C_{p_n} with p_j/p_∞ at each of the wing pressure orifices influenced by the jet shock for all the propulsive jets tested. Typical curves taken from the data of figure 13 from the orifices located at $x/D_j = 7.63$ are presented in figure 14 for the purpose of discussion. The rapid C_{p_n} drop in figure 14 happens when the point of intersection of the jet shock on the wing passes over the orifice as it moves downstream when p_j/p_∞ is increased. Figure 14 also shows that the C_{p_n} drop takes place at approximately the same values of p_j/p_∞ for the air and the $H_2 + CO_2$ jets while for the helium jet it takes place at greater values of p_j/p_∞ . This difference in C_{p_n} must be an effect of γ on the location of the jet shock for the same reasons as previously explained in the case for the exit shock. Also, as in the case for the exit shock, the effect of γ on the location of the jet shock is an increasing one with an increase in p_j/p_∞ because the difference in the variation of C_{p_n} between the helium jet and the other propulsive jets tested is greater in figure 14(a) than it is in figure 14(b). From the results of these tests as presented in figures 13 and 14, it appears that both p_j/p_∞ and γ will affect C_{p_n} as influenced by the jet shock while the exhaust parameters of density and velocity do not.

Effect of γ in relation to p_j/p_∞ on pressure coefficients.-
Figure 15 presents the chordwise variation of C_{p_n} on the wing at 1.40 D_j spanwise from the nacelle center line for both the $H_2 + CO_2$ and helium propulsive jets at two values of jet-exit static-pressure ratios. The chordwise profiles of C_{p_n} at $p_j/p_\infty = 4$ in figure 15(a) for both the propulsive jets presented were essentially the same. This similarity indicates that the difference in γ between these two propulsive jets had little or no effect on the C_{p_n} profile at $p_j/p_\infty = 4$. However, at $p_j/p_\infty = 8$, as presented in figure 15(b), a variation in the C_{p_n} profile is shown in the near vicinity of the intersection on the wing of both the exit shock and the jet shock. This variation, however, can be considered minor in relation to the overall C_{p_n} profile as determined by p_j/p_∞ . Also, the differences are in the direction that would be expected from figure 13, reference 4.

Effect of temperature on pressure coefficients.- It is shown in table I that the hot jet (hydrogen burned in air) had an absolute temperature that was approximately six times greater than the temperature of the cold jets tested. However, the hot-jet test was limited to a range of jet-exit static-pressure ratio (p_j/p_∞ of about 4) as can be seen in figure 5. The values of C_{p_n} for the hot-jet test as presented in figures 11 and 13 at $p_j/p_\infty = 4$ for each orifice position are essentially the same as those for the cold jets tested. This indicates that temperature itself had little or no effect on C_{p_n} for the pressure range tested. However, it is well known that temperature will affect the value of γ , and as shown in figure 15, γ has an increasing influence on the values of C_{p_n} with an increase in p_j/p_∞ .

CONCLUSIONS

Within the limits of the present static-pressure surveys on a flat surface wing located in the vicinity of a sonic propulsive jet that was operated with four types of exhaust jets at a free-stream Mach number of 1.80, the results may be summarized as follows:

1. The exhaust parameters of jet-exit static-pressure ratio and γ affected the pressure distribution on the wing associated with jet interference.
2. The exhaust parameter of jet-exit static-pressure ratio affected the wing pressure distribution in a major way while the exhaust parameter of the ratio of specific heats had only a minor effect.
3. The addition of temperature in the propulsive jet exhaust at a jet-exit static-pressure ratio of 4 had little or no effect on the pressure distribution on the wing associated with jet interference.
4. The exhaust parameters of exit velocity and density had little or no effect on the pressure distribution on the wing associated with jet interference.

Langley Aeronautical Laboratory,
National Advisory Committee for Aeronautics,
Langley Field, Va., April 17, 1956.

REFERENCES

1. Bressette, Walter E.: Investigation of the Jet Effects on a Flat Surface Downstream of the Exit of a Simulated Turbojet Nacelle at a Free-Stream Mach Number of 2.02. NACA RM L54E05a, 1954.
2. Englert, Gerald W., Wasserbauer, Joseph F., and Whalen, Paul: Interaction of a Jet and Flat Plate Located in an Airstream. NACA RM E55G19, 1955.
3. Bressette, Walter E., and Leiss, Abraham: Investigation of Jet Effects on a Flat Surface Downstream of the Exit of a Simulated Turbojet Nacelle at a Free-Stream Mach Number of 1.39. NACA RM L55L13, 1956.
4. Love, Eugene S., and Grigsby, Carl E.: Some Studies of Axisymmetric Free Jets Exhausting From Sonic and Supersonic Nozzles Into Still Air and Into Supersonic Streams. NACA RM L54L31, 1955.
5. Faget, Maxime A., Watson, Raymond S., and Bartlett, Walter A., Jr.: Free-Jet Tests of a 6.5-Inch-Diameter Ram-Jet Engine at Mach Numbers of 1.81 and 2.00. NACA RM L50L06, 1951.
6. Ciepluch, Carl C., Velie, Wallace W., and Burley, Richard R.: Afterburner Performance With Combustion-Chamber Lengths from 10 to 62 Inches at Several Afterburner-Inlet Temperatures. NACA RM E55K09, 1956.

TABLE I

VALUES OF PROPULSIVE JET EXHAUST PARAMETERS

Type of propulsive jet tested	M_j	ρ , lb/cu ft (*)	γ	$\frac{R, \text{ft-lb}}{\text{lb } ^\circ\text{R}}$	$T, ^\circ\text{R}$	V_j , ft/sec
Hot jet (hydrogen and air)	1	0.0434	1.27	59	3,300	2,820
Air jet	1	.324	1.40	53.3	520	1,120
Helium jet	1	.0440	1.66	386	520	3,275
Hydrogen and carbon dioxide jet	1	.0435	1.397	374	520	2,955

$$\frac{p_j^*}{p_\infty} = 4.$$

TABLE II

VALUES OF JET-OFF PRESSURE COEFFICIENTS FOR
ALL WING ORIFICE POSITIONS

Orifice ordinates		C_{pf}	Orifice ordinates		C_{pf}
x/D_j	y/D_j		x/D_j	y/D_j	
10.76	0	0.001	10.76	4.17	0.016
9.72		.019	9.72		.031
8.68		.026	8.68		-.077
7.63		.028	7.63		-.042
6.59		.036	6.59		-.113
5.55		-.094	5.55		-.100
4.51		-.070	4.51		-.056
3.47		-.101	3.47		-.034
2.43		-.091	2.43		-.009
1.39		-.047	1.39		-.005
.35		-.018	.35		-.002
-.69		-.006			
10.76	1.40	0.004	10.76	6.94	-0.084
9.72		.023	9.72		-.075
8.68		.033	8.68		-.038
7.63		.036	7.63		-.035
6.59		-.020	6.59		-.036
5.55		-.112	5.55		-.036
4.51		-.081	4.51		-.030
3.47		-.117	3.47		-.010
2.43		-.070	10.76	11.11	-0.030
1.39		-.035	9.72		-.015
.35		-.009	8.68		-.010
-.69		.000	7.63		-.010



L-86661
Figure 1.- Photograph of the nacelle mounted beneath the flat-surface
wing in the 27- by 27-inch preflight-jet nozzle.

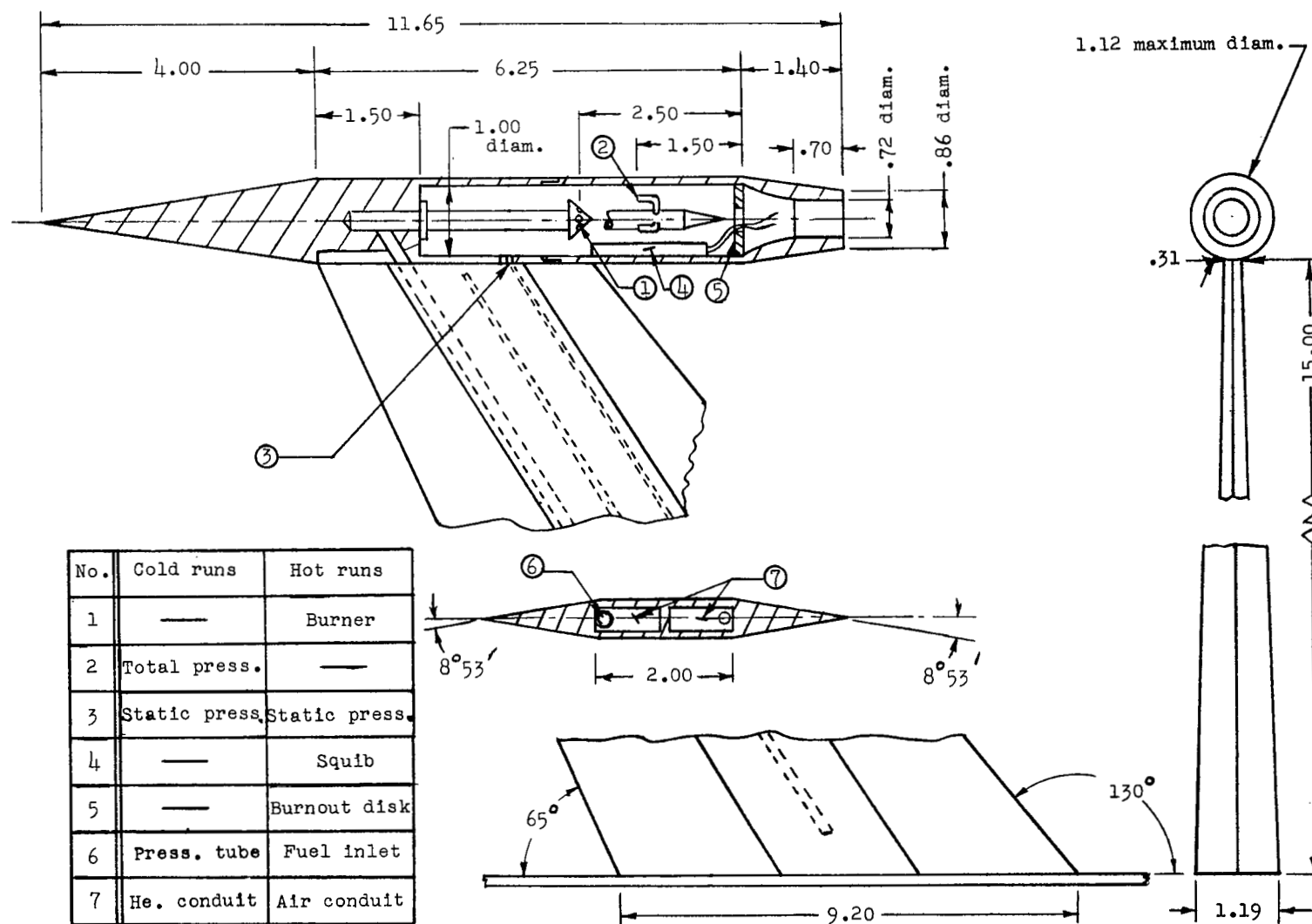


Figure 2.- Schematic diagram of nacelle. All dimensions are in inches.

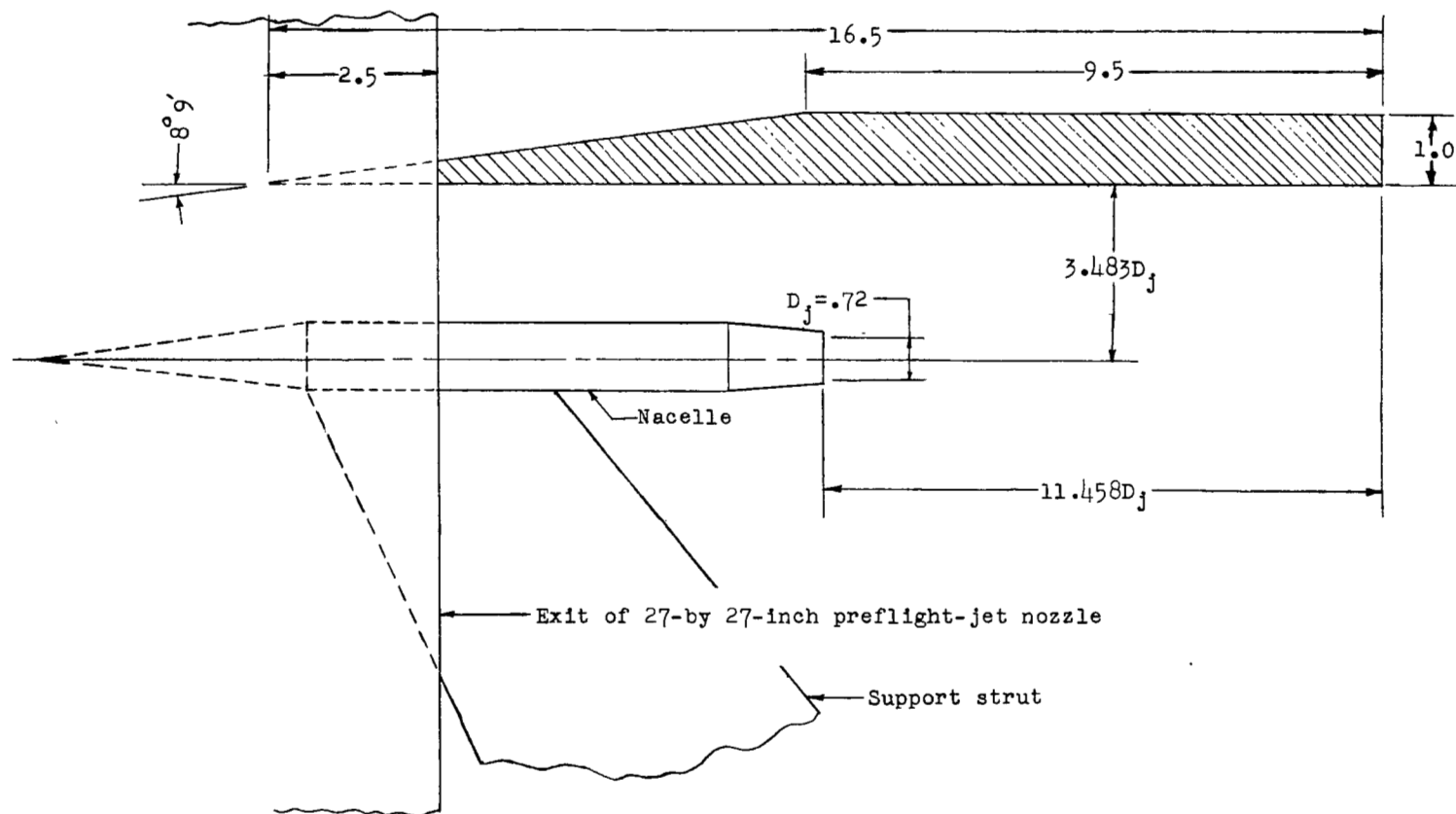


Figure 3.- Arrangement of the nacelle relative to the exit of the 27-by 27-inch preflight-jet nozzle and wing. Dimensions are in inches except as otherwise noted.

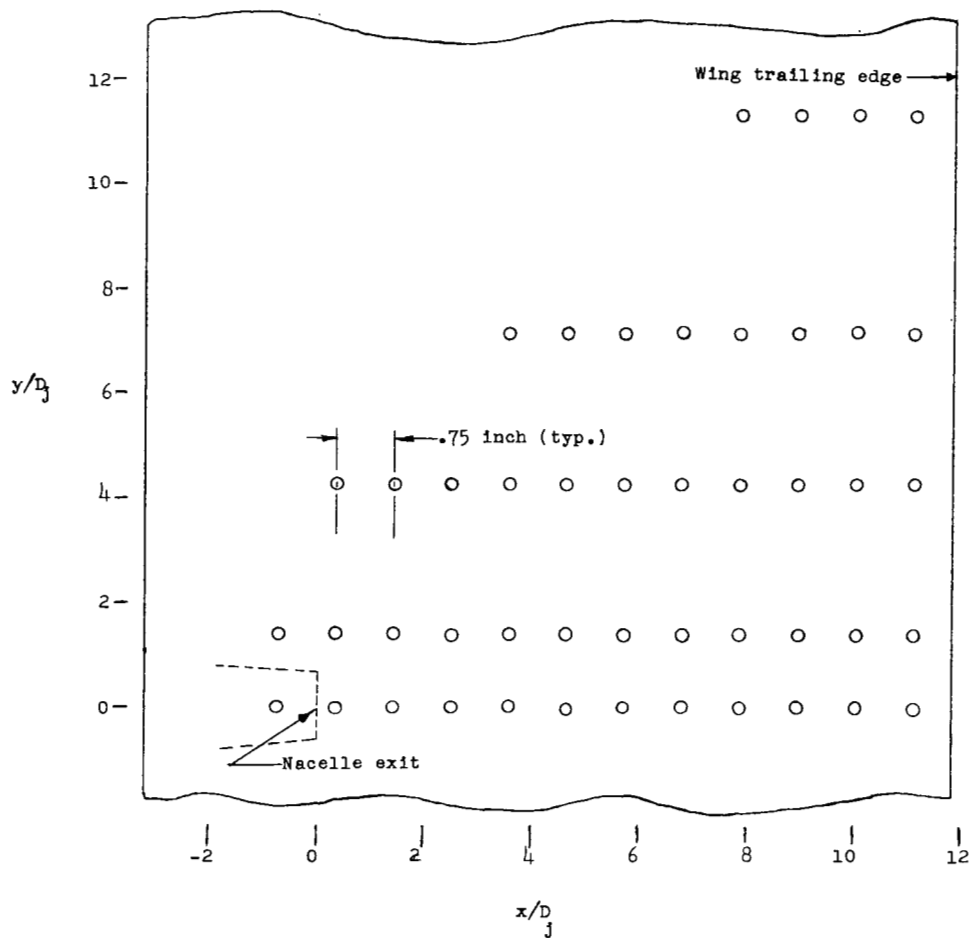


Figure 4.- Location of the wing static-pressure orifices.

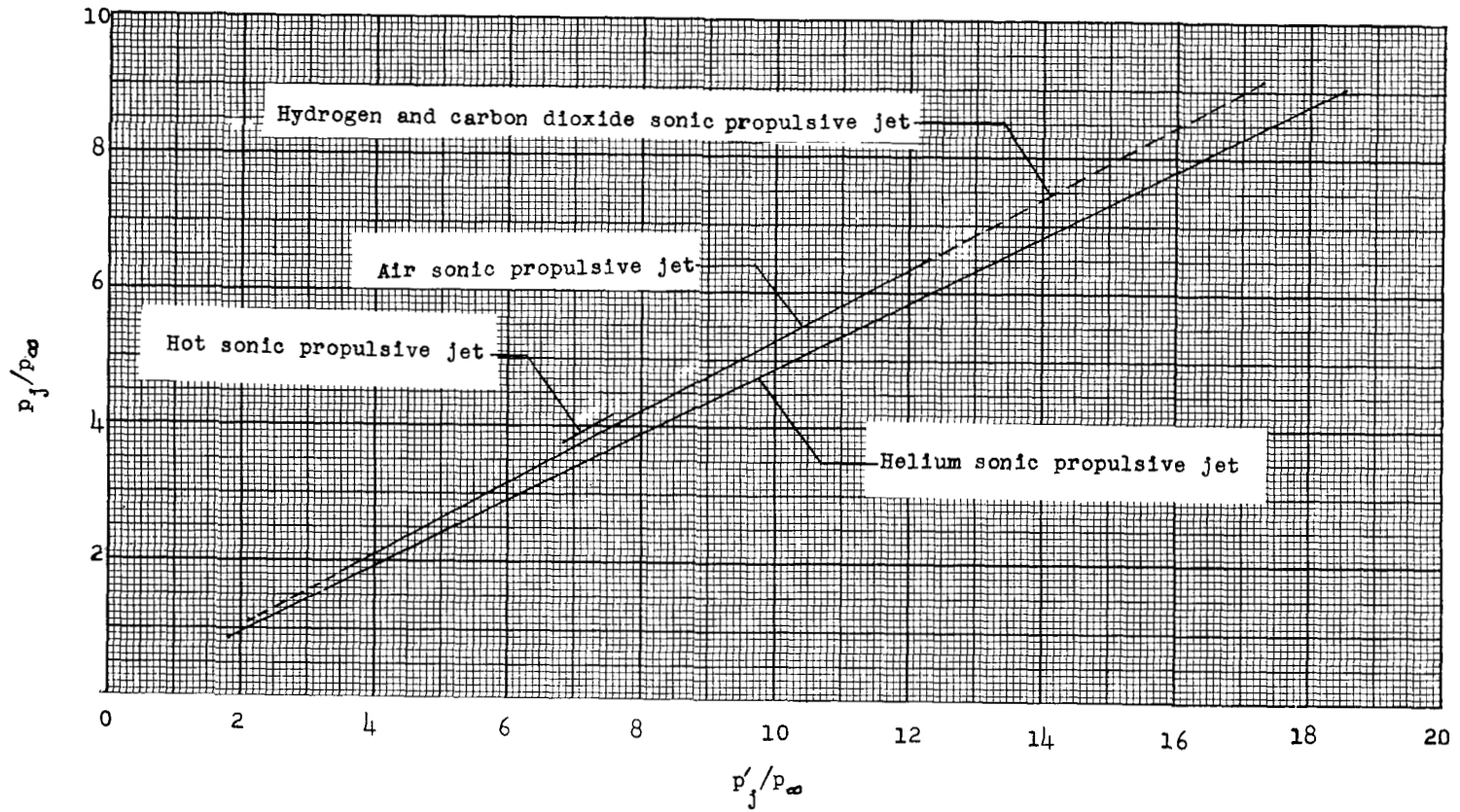


Figure 5.- Variation of jet-exit static-pressure ratio with jet-exit total-pressure ratio for all propulsive jets tested.

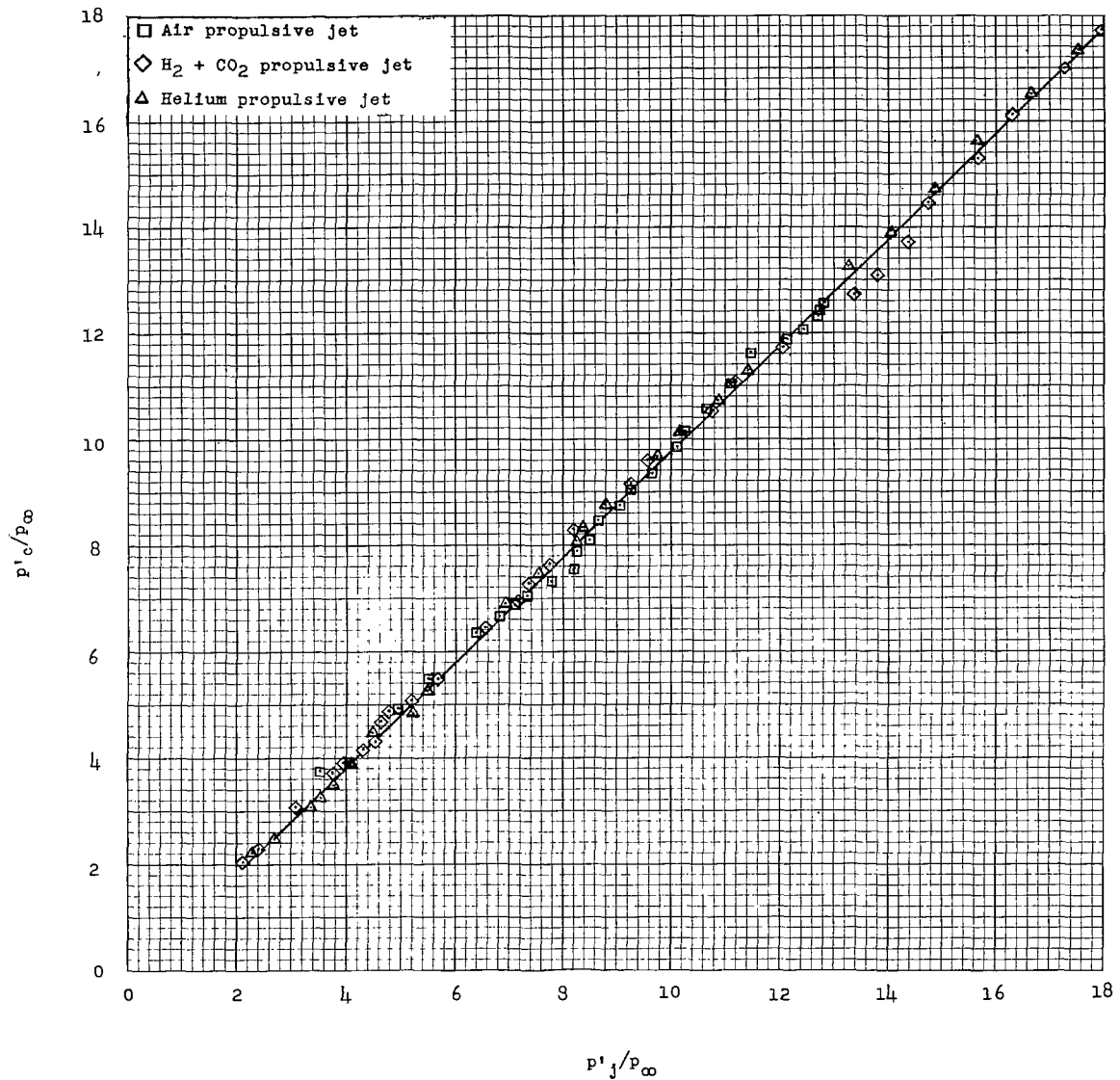
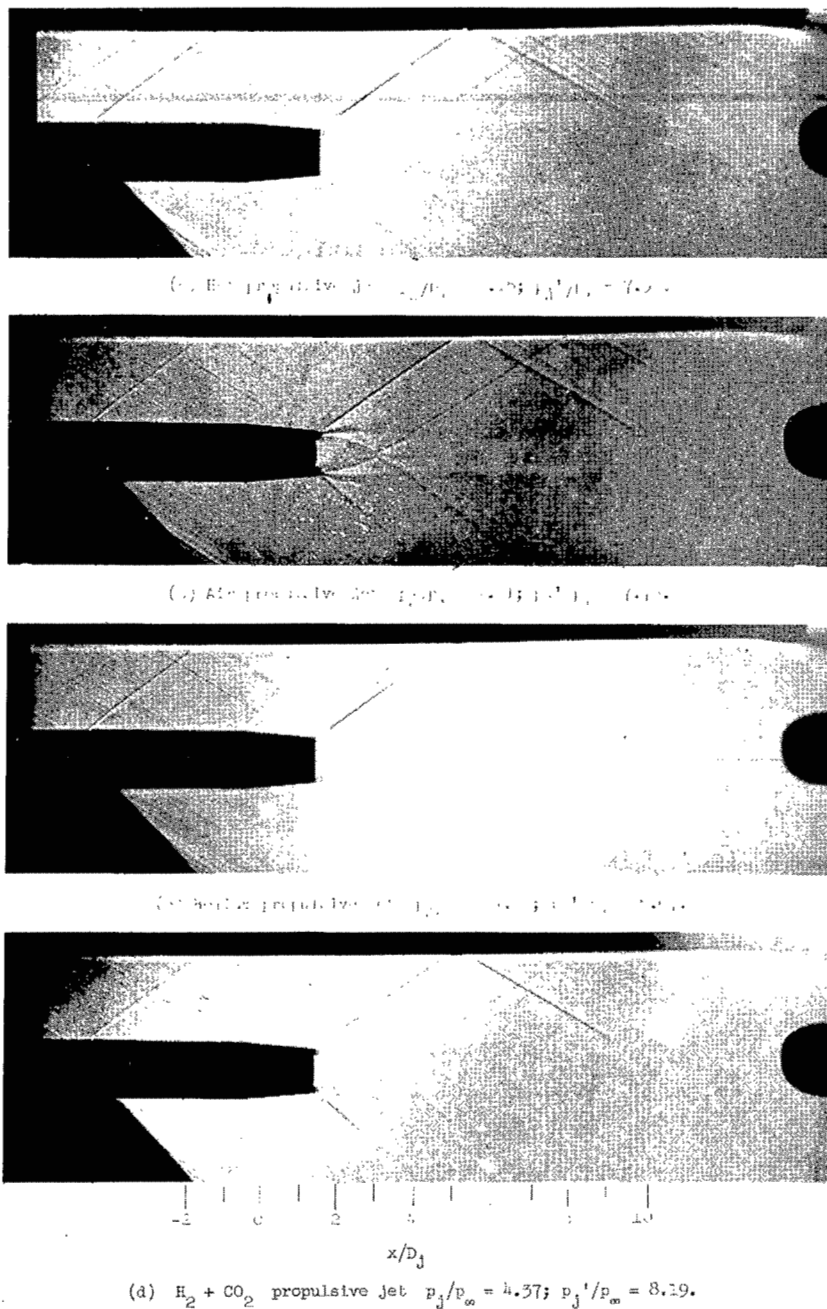


Figure 6.- Variation of measured nacelle-chamber total-pressure ratio with calculated jet-exit total-pressure ratio from thrust measurements.



L-92483

Figure 7.- Shadowgraph pictures of the flow field about the nacelle exit for the four types of propulsive jets tested.

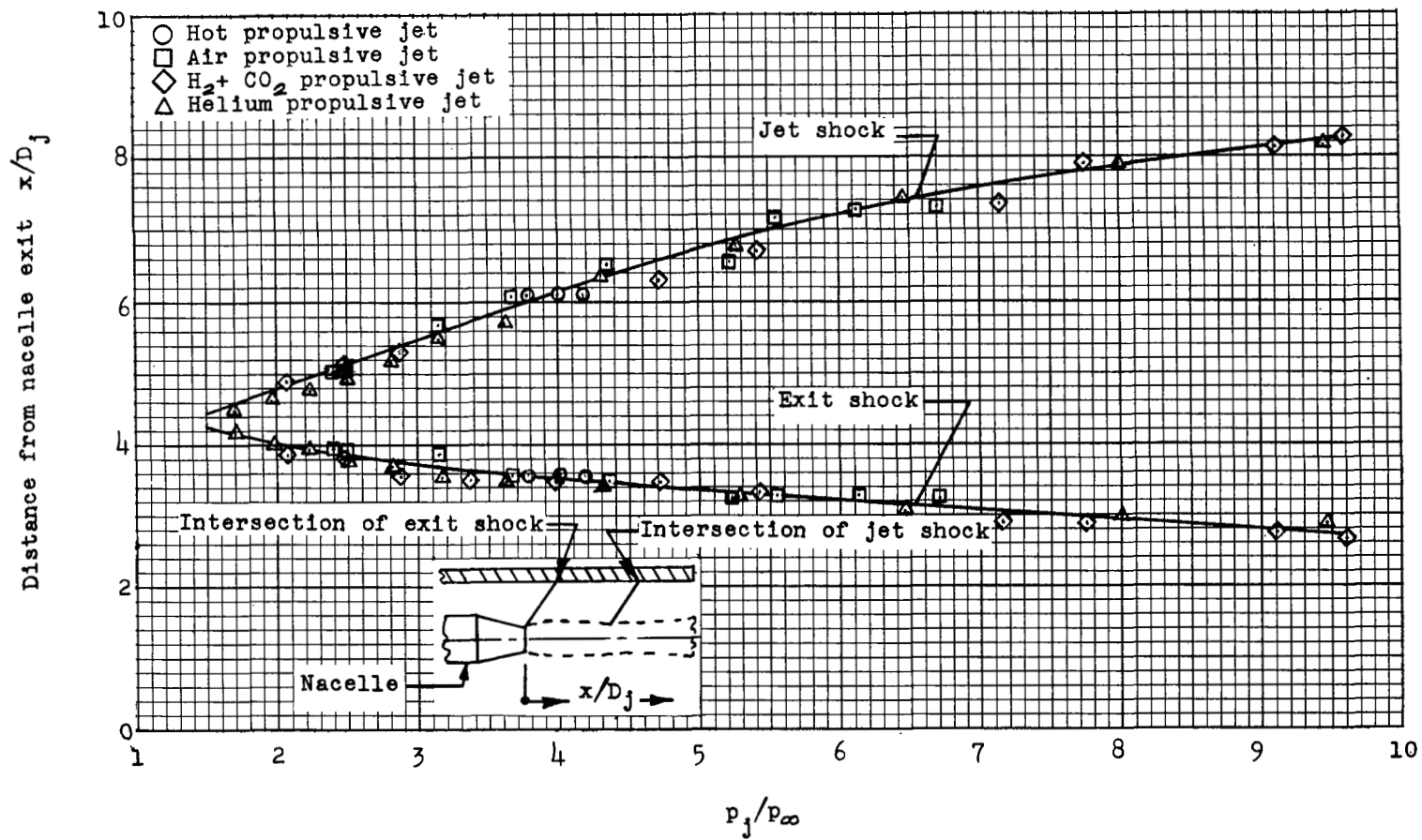


Figure 8.- Point of intersection on wing of exit and jet shock waves as measured from shadowgraph pictures.

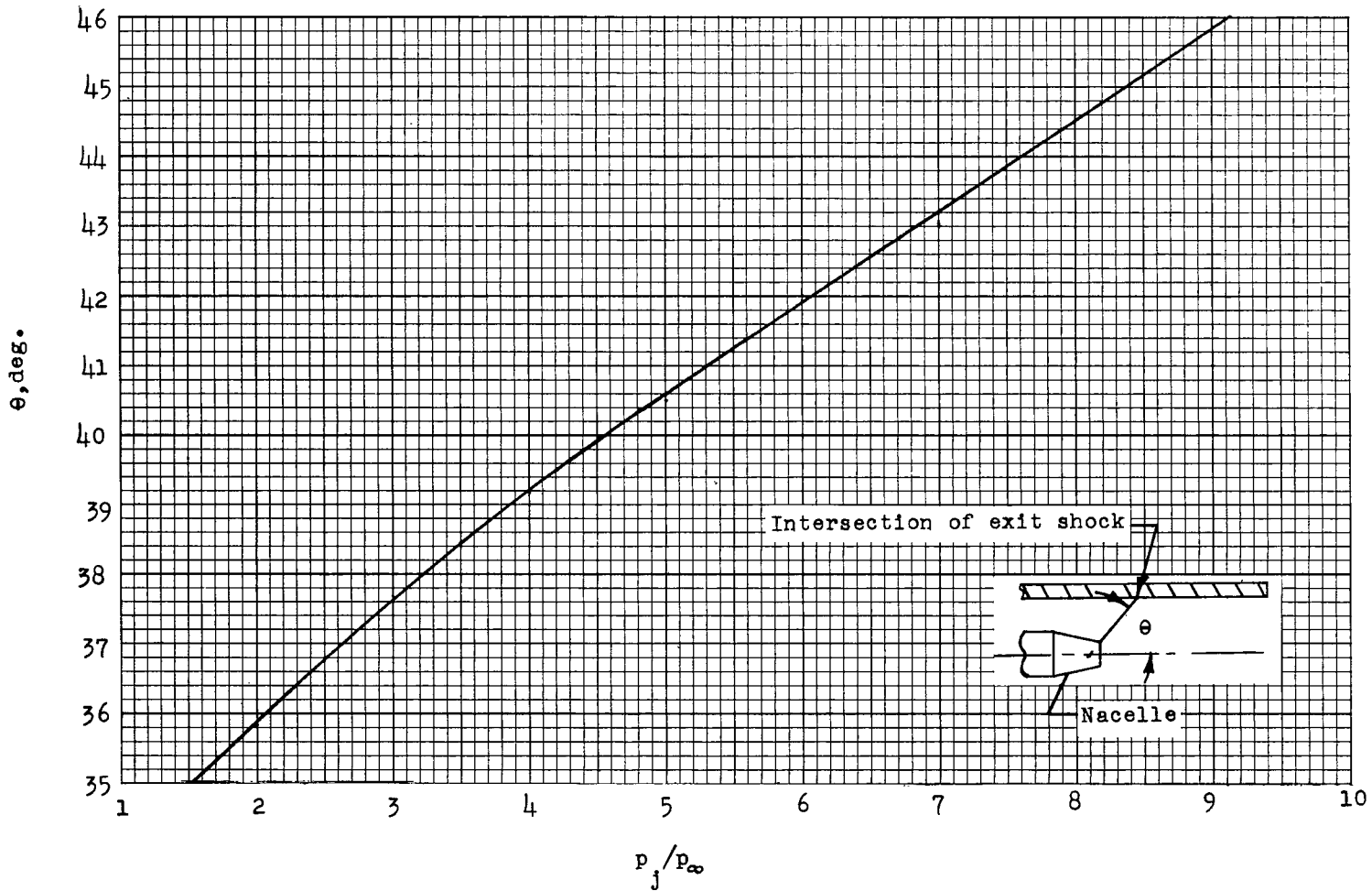


Figure 9.- Variation of the angle between the nacelle center line and a line drawn from the point of intersection on the wing of the exit shock wave and the nacelle exit with jet-exit static-pressure ratio.

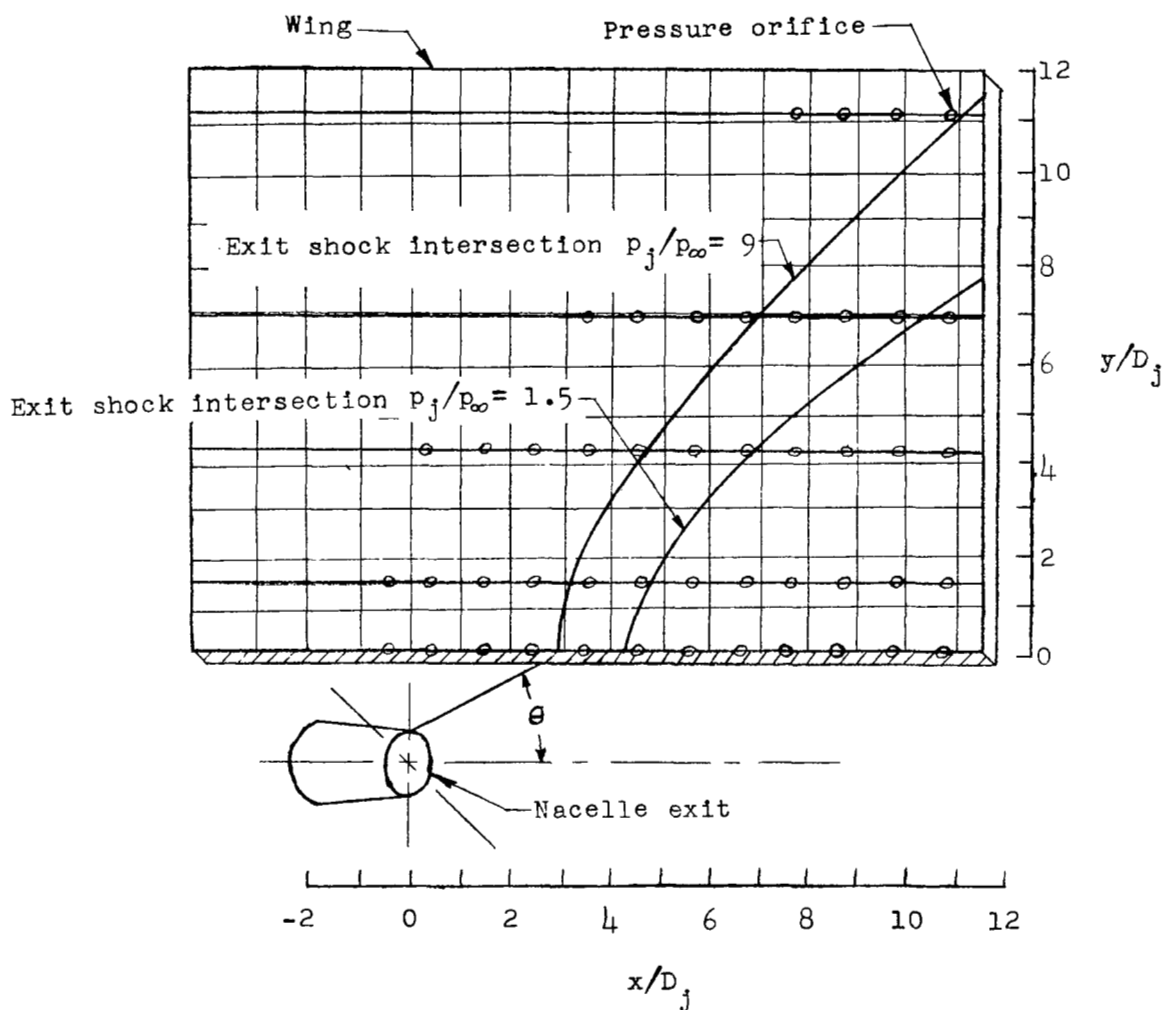
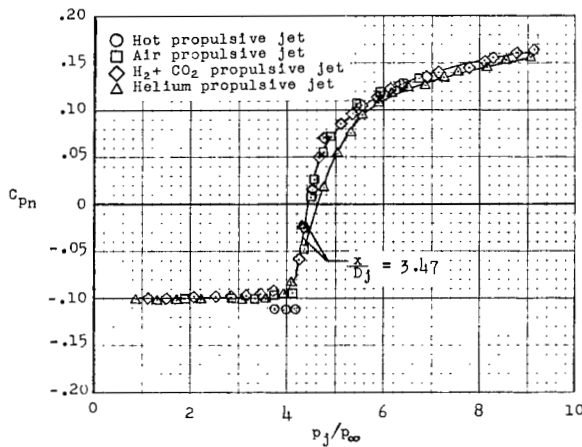
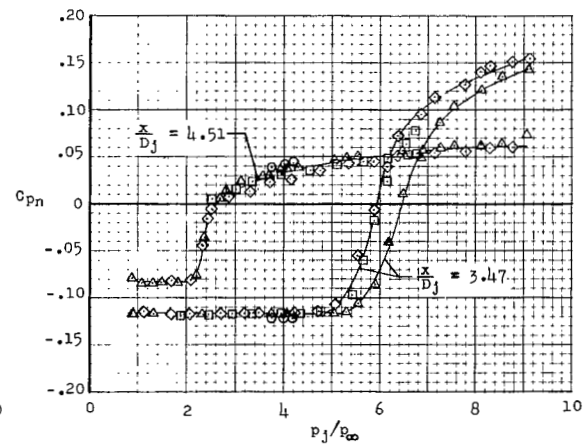


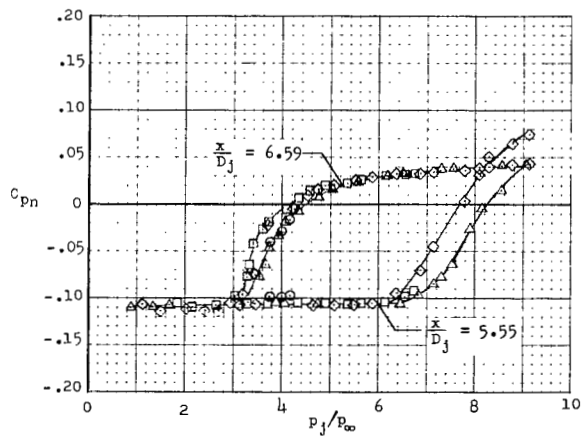
Figure 10.- Intersection of exit-shock wave on flat-plate wing.



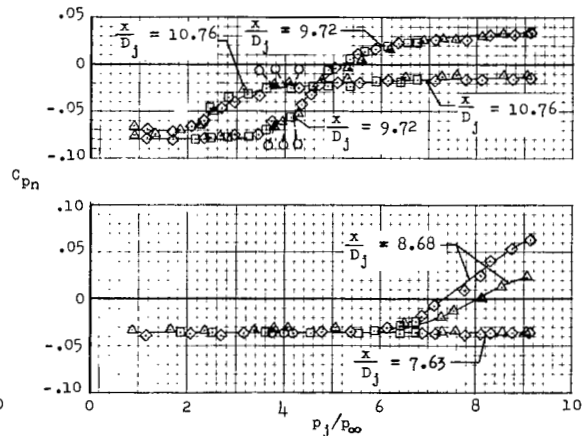
(a) Along the nacelle center line.



(b) $1.40D_j$ spanwise from the nacelle center line.

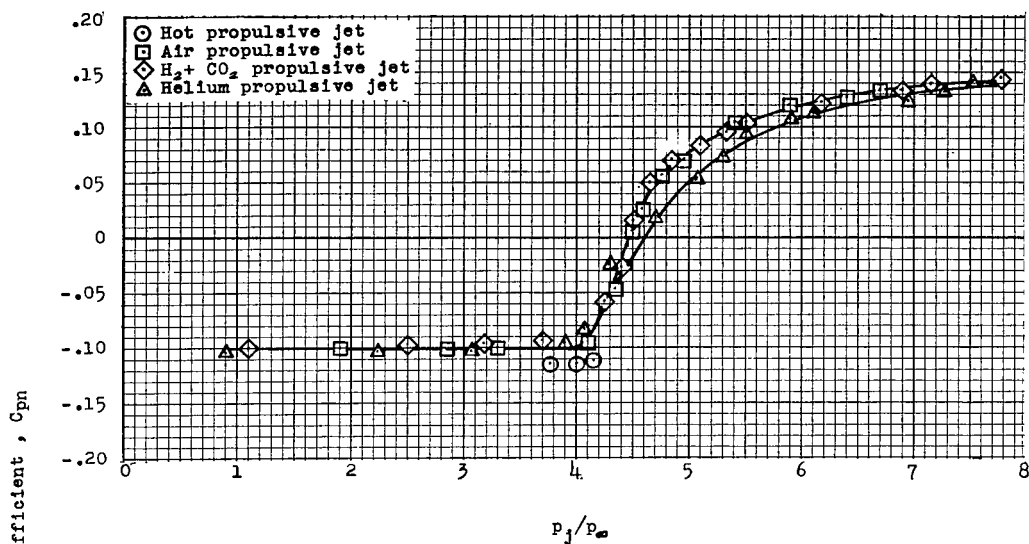


(c) $4.17D_j$ spanwise from the nacelle center line.



(d) $6.94D_j$ spanwise from the nacelle center line.

Figure 11.- Variation of jet-on pressure coefficients with jet-exit static-pressure ratio for the orifices influenced by the exit-shock for all propulsive jets tested.



(a) At nacelle center line.

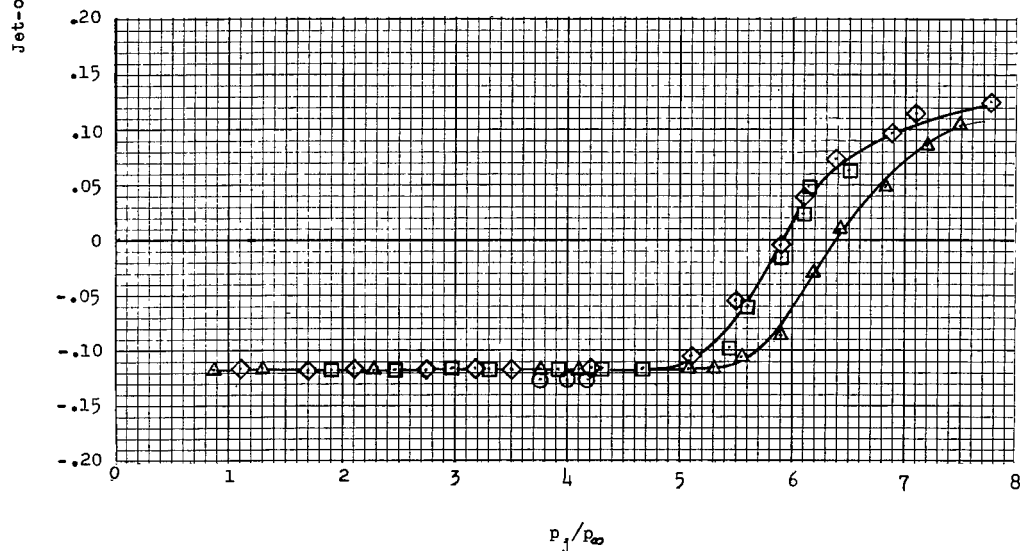
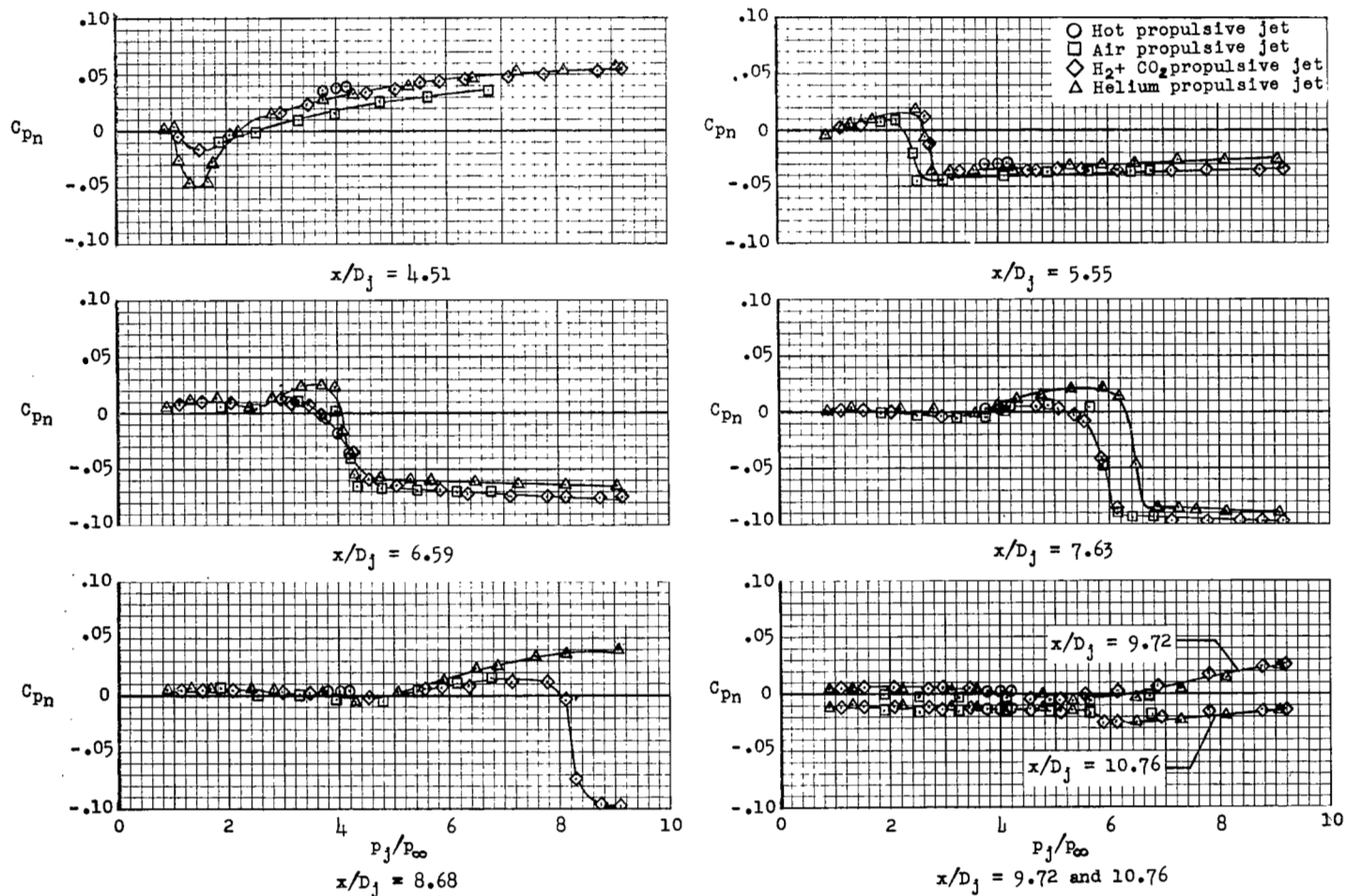
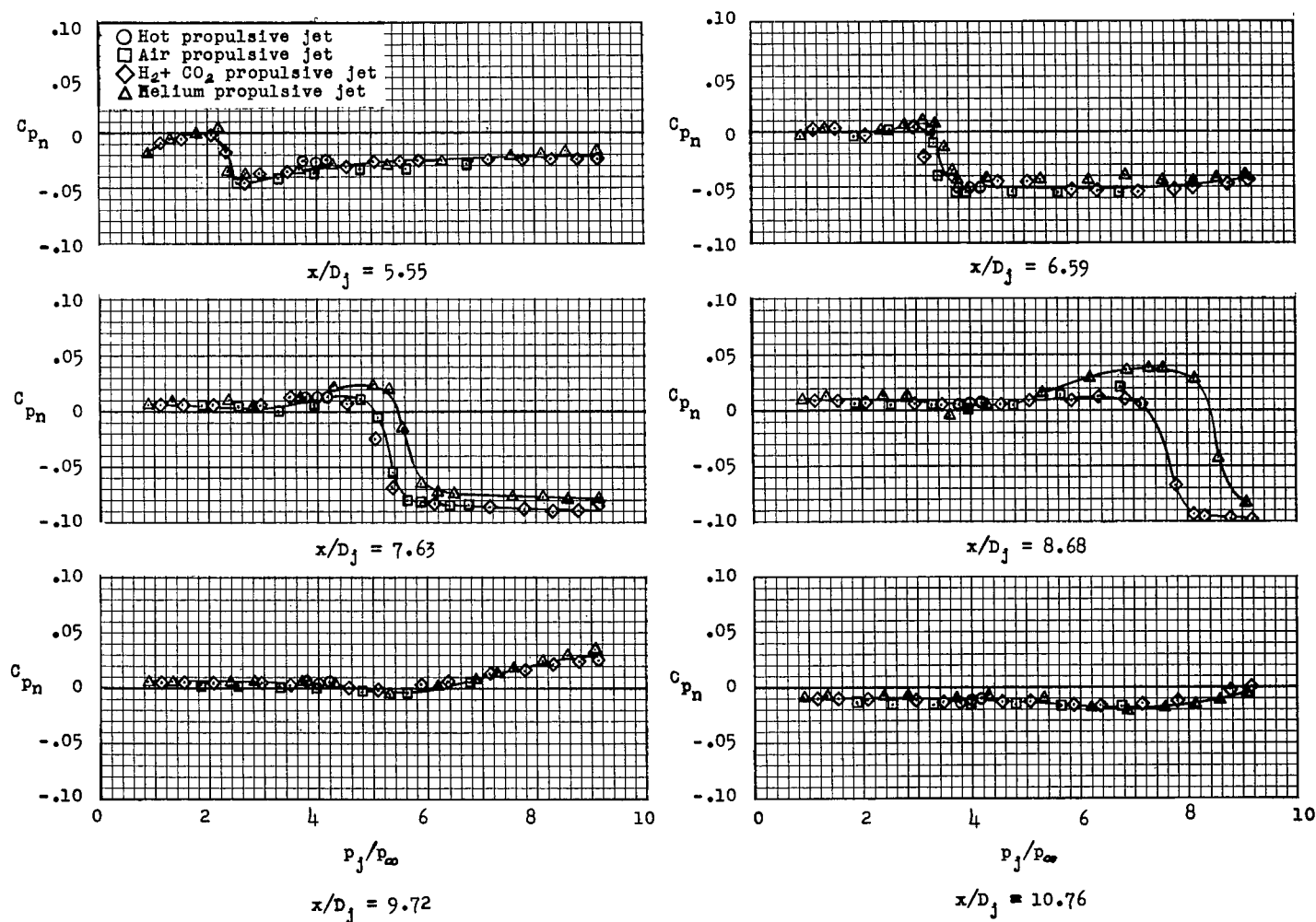
(b) At $1.4OD_j$ spanwise from nacelle center line.

Figure 12.- Typical curves from the data of figure 11 of the variation of jet-on pressure coefficient with jet-exit static-pressure ratio for the orifices located 3.47 jet diameters behind the exit for all the propulsive jets tested.



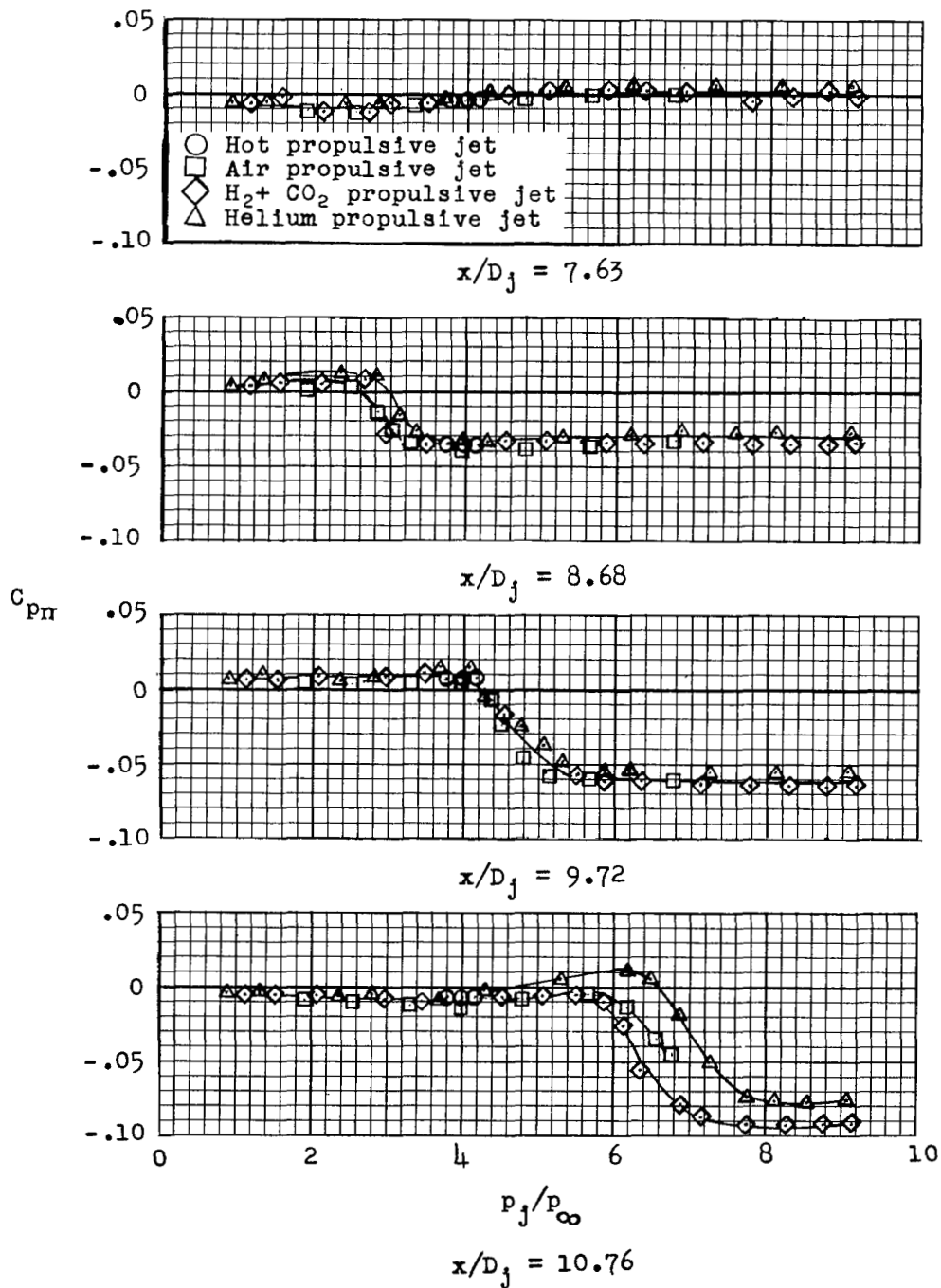
(a) Along the nacelle center line.

Figure 13.- Variation of jet-on pressure coefficient with jet-exit static-pressure ratio for the orifices influenced by the jet shock for all the propulsive jets tested.



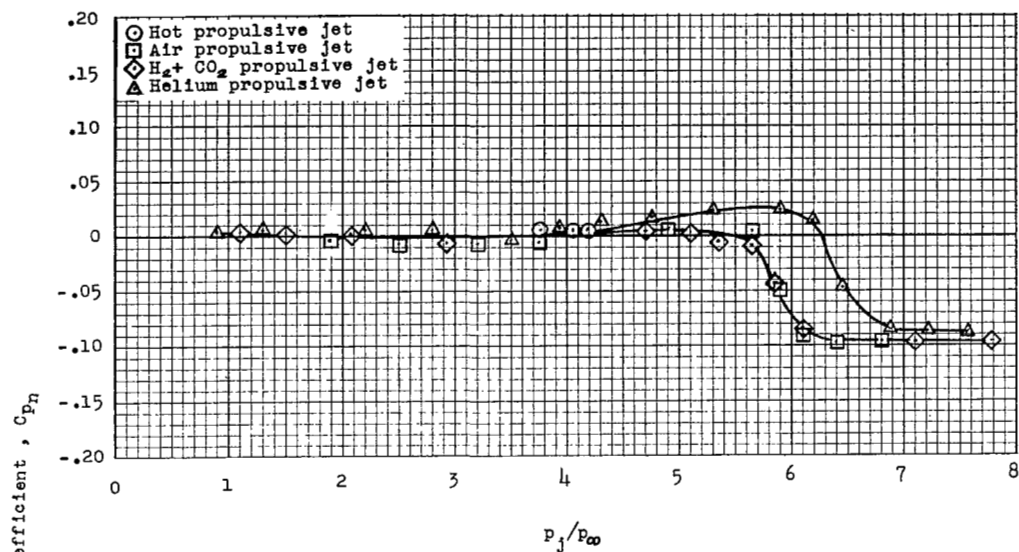
(b) $1.40D_j$ spanwise from nacelle center line.

Figure 13.- Continued.



(c) $4.17D_j$ spanwise from the nacelle center line.

Figure 13.- Concluded.



(a) At nacelle center line.

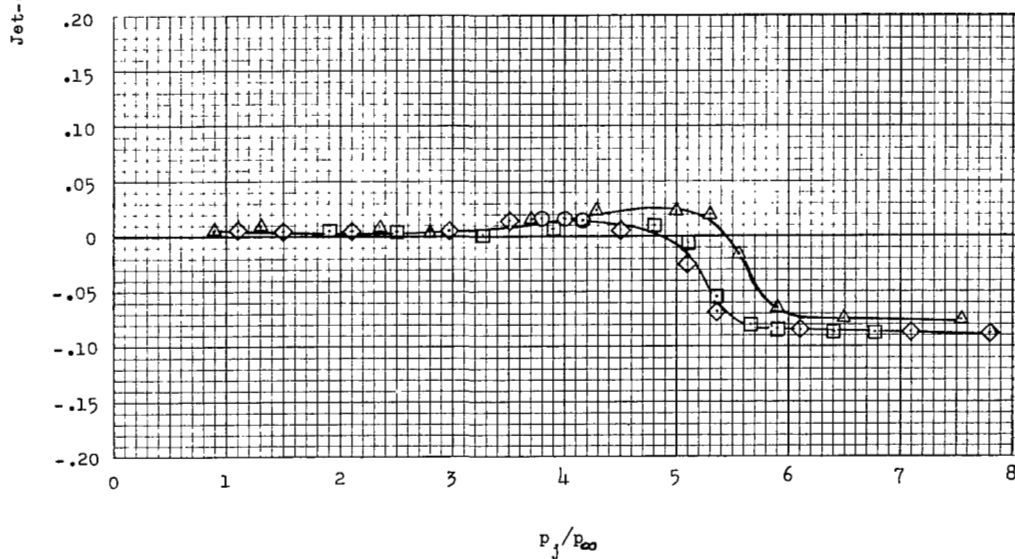
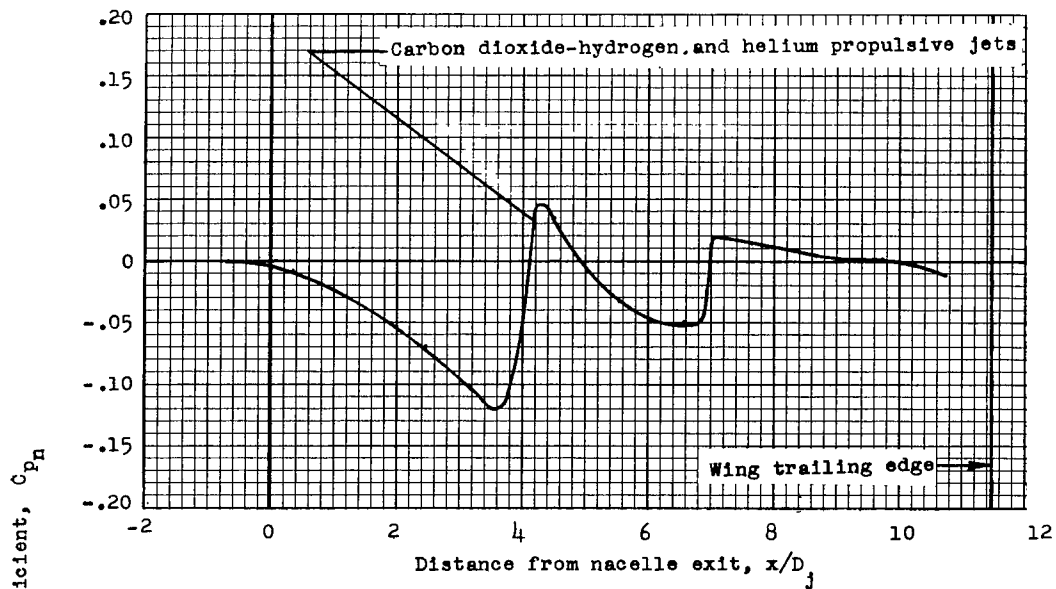
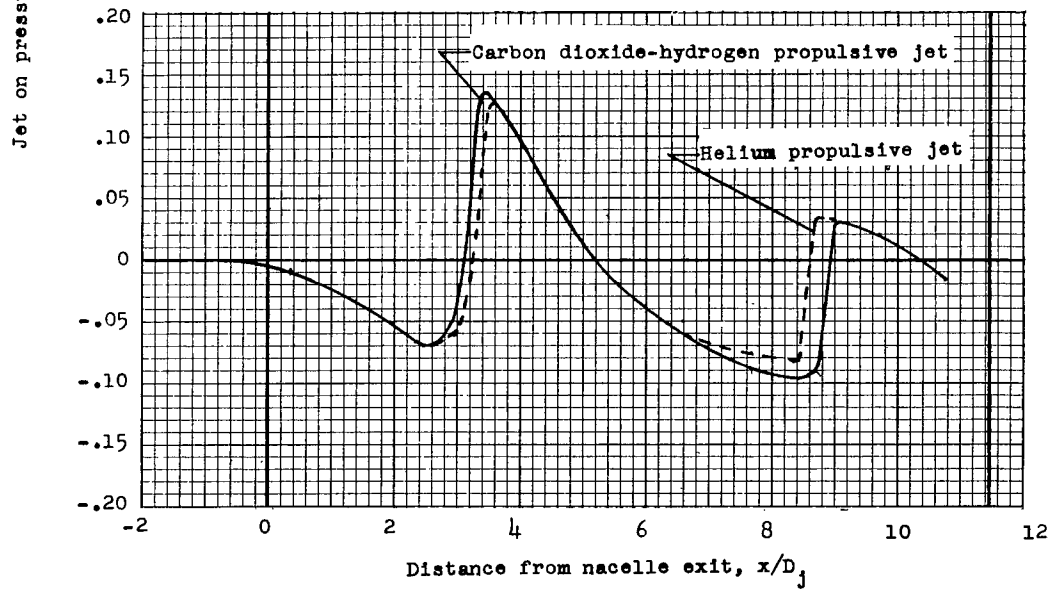
(b) At $1.40D_j$ spanwise from nacelle center line.

Figure 14.- Typical curves from the data of figure 13 of the variation of jet-on pressure coefficient with jet-exit static-pressure ratio for the orifices located 7.63 jet diameters behind the exit for all propulsive jets tested.



(a) $p_j/p_\infty = 4$.



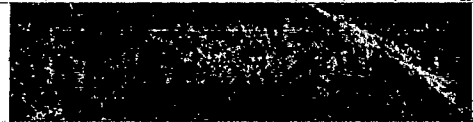
(b) $p_j/p_\infty = 8$.

Figure 15.- Chordwise variation of jet-on pressure coefficients at $1.40D_j$ spanwise from the nacelle center line for both the mixture of carbon dioxide-hydrogen and helium propulsive jets at two values of jet-exit static-pressure ratio.

NASA Technical Library



3 1176 01437 2248



~~CONFIDENTIAL~~